Metal Binding Sites in Proteins: Identification and Characterization by Paramagnetic NMR Relaxation†

Malene Ringkjøbing Jensen,‡ Gitte Petersen,§ Conni Lauritzen,§ John Pedersen,§ and Jens J. Led*,‡

Department of Chemistry, University of Copenhagen, Universitetsparken 5, DK-2100 Copenhagen Ø, Denmark, and Unizyme Laboratories A/S, Dr. Neergaardsvej 17, DK-2970 Hørsholm, Denmark

Received May 3, 2005; Revised Manuscript Received June 21, 2005

ABSTRACT: A method is presented that allows the identification and quantitative characterization of metal binding sites in proteins using paramagnetic nuclear magnetic resonance spectroscopy. The method relies on the nonselective longitudinal relaxation rates of the amide protons and their dependence on the paramagnetic metal ion concentration and the pH, and on the three-dimensional structure of the protein. The method is demonstrated using *Escherichia coli* thioredoxin as a model protein and Ni^{2+} as the paramagnetic metal ion. Through a least-squares analysis of the relaxation rates, it is found that Ni^{2+} binds to a series of specific sites on the surface of thioredoxin. The strongest binding site is found near the N-terminus of the protein, where the metal ion is coordinated to the free NH_2 group of the N-terminal serine residue and the side chain carboxylate group of the aspartic acid residue in position 2. In addition, Ni^{2+} binds specifically but more weakly to the surface-exposed side chain carboxylate groups of residues D10, D20, D47, and E85.

Metal ions are essential for the structure and function of many biological proteins. Precise knowledge of the metal−protein interactions is, therefore, necessary in order to understand the function of these proteins at the molecular level. In many metalloproteins the metal ion is bound tightly to the protein, and the structure of the binding site can be determined accurately by X-ray crystallography. In other proteins, however, the metal ions bind only loosely and temporarily, as in the case of many enzymes that use metal ions as cofactors or in the case of proteins that require metal ions for temporary stabilization or storage. For such proteins, the specific metal binding sites are often poorly characterized or even unknown. Still, a precise knowledge of the metal−protein interaction, including the location of the metal binding site and its binding characteristics, may be necessary in order to elucidate the function and the functional mechanism of the metal-dependent proteins.

The biological importance of metal−protein interactions is emphasized by the large number of studies that have been made in order to predict or identify possible metal binding sites in proteins and design new sites (*1*−*10*). Also, it is emphasized by the number of reviews covering the topic (*11*−*16*). In such studies, paramagnetic metal ions are particularly useful because of the strong interactions between the unpaired electrons of the metal ions and the nuclei of the protein. These interactions, which can be determined precisely by nuclear magnetic resonance (NMR)[1] spectroscopy, provide detailed information about the metal−protein interactions at the atomic level. Therefore, paramagnetic NMR has been used to identify metal binding sites and functional regions on protein surfaces (*17*−*23*) and to obtain structural information from the long-range electron nucleus interactions (*24*−*31*). Normally, paramagnetic metal ions such as Fe^{2+}, Cu^{2+}, Ni^{2+}, Mn^{2+}, and Co^{2+} or lanthanide ions are being used in these studies, either as the aqua complex or as a small organic complex, binding either to the native protein directly or to a metal binding tag attached to the protein. Also organic spin labels have been used in paramagnetic NMR studies of protein structures (*32*−*35*).

Despite the usefulness of paramagnetic metal ions in NMR studies of metal−protein interactions, a quantitative interpretation of the experimental data is, in general, less straightforward. Thus, the experimental paramagnetic NMR data are often complicated functions of the parameters that characterize the metal−protein interactions, such as the dissociation constants, the ligand exchange rates, and the geometric and electronic structures of the binding sites. A detailed interpretation of the experimental data can, therefore, be difficult and may require a large and versatile data set to determine all of the involved parameters. Consequently, paramagnetic NMR data are often used in a semiquantitative manner, the interpretation being made on the basis of a reduced data set using a series of approximations.

Here, we present an NMR approach that allows the identification and quantitative characterization of all the sites

† This work was financially supported by the Danish Natural Science Research Council, J. Nos. 9400351, 9801801, 51-00211, 21-01-0545, and 21-04-0519, Carlsbergfondet, J. No. 1624/40, Novo Nordisk Fonden, J. No. 2003-11-28, and Villum Kann Rasmussen Fonden, J. No. 8.12.2003.

* To whom correspondence should be addressed. Telephone: (+45) 35 32 03 02. Fax: (+45) 35 32 03 22. E-mail: led@kiku.dk.

‡ University of Copenhagen.

§ Unizyme Laboratories A/S.

[1] Abbreviations: NMR, nuclear magnetic resonance; HSQC, heteronuclear single-quantum coherence; *E. coli*, *Escherichia coli*; Trx, thioredoxin; IPTG, isopropyl 1-thio-β-galactopyranoside; IR, inversion recovery.

10.1021/bi0508136 CCC: $30.25 © 2005 American Chemical Society
Published on Web 07/28/2005

in a protein that interact specifically with the applied paramagnetic metal ion. The method relies on the nonselective longitudinal relaxation rates of the amide protons as a function of the metal ion concentration and the pH, and on the three-dimensional structure of the protein. Although the method is computationally intensive, it is conceptually simple. Thus, using the distance information provided by the relaxation rates and the three-dimensional structure of the protein determined by NMR or X-ray crystallography, the metal binding sites can be located and their occupancies can be determined through a least-squares analysis of the relaxation data. The protein *Escherichia coli* (*E. coli*) thioredoxin (Trx) was used as the model protein (*36*), while Ni^{2+} was used as the paramagnetic metal probe.

THEORY

The exchange between the metal-free, diamagnetic form of Trx and a metal-bound, paramagnetic form of the protein is considered:

$$\mathrm{Trx} + \mathrm{M} \underset{k_{\mathrm{off}}}{\overset{k_{\mathrm{on}}}{\rightleftharpoons}} \mathrm{TrxM} \tag{1}$$

Here, M is a paramagnetic metal ion and k_{on} is the second-order rate constant for the complex formation, while k_{off} is the first-order rate constant for the complex dissociation. After a perturbation of the spin system, the time dependence of the longitudinal magnetizations, $M_d(t)$ and $M_p(t)$, in the diamagnetic and the paramagnetic site, respectively, is, in general, biexponential and is described by the McConnell equations for a two-site exchange system (*37*). Thus $M_d(t)$ is given by

$$M_d(t) = C_1 \exp(\lambda_1 t) + C_2 \exp(\lambda_2 t) + M_d^{\infty} \tag{2}$$

where M_d^{∞} is the equilibrium magnetization. Furthermore, the exponents, λ_1 and λ_2, and the preexponential constants, C_1 and C_2, are complex functions of the exchange rate, the fraction of the metal-bound protein, the magnetization, and the relaxation rates in the two sites, as described previously (*38*, *39*). However, under the experimental conditions applied here, it can be shown that λ_1 and λ_2 are negative and that $|\lambda_1|$ is significantly smaller than $|\lambda_2|$. Furthermore, $|C_1|$ is significantly larger than $|C_2|$ for all fractions of the metal-bound protein used here, making $M_d(t)$ single exponential to a good approximation (*39*). Thus, in the presence of an exchanging metal ion, the observed longitudinal relaxation rate, R_{1o}, of the signal corresponding to the metal-free form is given by (*38*, *39*)

$$R_{1o} = \frac{2R_{1d} + R_{1p} + k}{2} - \sqrt{\left(\frac{R_{1p} + k}{2}\right)^2 - k f_p R_{1p}} \tag{3}$$

Here, R_{1d} is the relaxation rate of the nucleus in the free diamagnetic complex, R_{1p} is the paramagnetic relaxation enhancement of the nucleus, and f_p is the fraction of the metal-bound protein. Finally, k is the rate of exchange between the two forms of the protein which is given by

$$k = k_{\mathrm{on}}[\mathrm{M}] + k_{\mathrm{off}} = \frac{k_{\mathrm{off}}}{1 - f_p} \tag{4}$$

The paramagnetic relaxation enhancement is given by (*40*)

$$R_{1p} = \frac{2}{15}\left(\frac{\mu_0}{4\pi}\right)^2 S(S+1) g_e^2 \mu_B^2 \gamma_I^2 r^{-6} \left[\frac{3\tau_{c,1}}{1 + \omega_I^2 \tau_{c,1}^2} + \frac{7\tau_{c,2}}{1 + \omega_S^2 \tau_{c,2}^2}\right] \tag{5}$$

Here, μ_0 is the permeability of free space, S is the electron spin quantum number, and g_e is the electron g-factor. Furthermore, μ_B is the Bohr magneton, γ_I is the gyromagnetic ratio of the nuclear spin I, and r is the distance between the metal ion and the nucleus. Finally, ω_I and ω_S are the Larmor frequencies of the nuclear spin I and the electron spin S, respectively. The correlation times, $\tau_{c,1}$ and $\tau_{c,2}$, can be written as

$$\tau_{c,1} = (\tau_r^{-1} + R_{1e} + k)^{-1} \tag{6}$$

$$\tau_{c,2} = (\tau_r^{-1} + R_{2e} + k)^{-1} \tag{7}$$

where R_{1e} and R_{2e} are the longitudinal and the transverse electron relaxation rates, respectively, while τ_r is the correlation time for the rotational reorientation of the complex.

Equation 5 is formally correct only if (1) the point dipole approximation applies, i.e., the unpaired electrons are located at the metal ion, (2) the g-tensor is isotropic, and (3) no zero-field splitting is present. For the paramagnetic Ni^{2+} ion used in the study here, the effect of the anisotropy of the g-tensor (*41*−*43*) and the zero-field splitting (*44*, *45*) on the paramagnetic relaxation enhancement is small and can be neglected in the analysis.

In the fast-exchange regime of the longitudinal relaxation ($R_{1p} \ll k$), eq 3 reduces to

$$R_{1o} = R_{1d} + f_p R_{1p} \tag{8}$$

that is, the observed longitudinal relaxation rate still depends on R_{1p} and can thereby give information about the metal−nucleus distances (see eq 5). However, in the slow-exchange regime of the longitudinal relaxation ($R_{1p} \gg k$) eq 3 becomes

$$R_{1o} = R_{1d} + f_p k \tag{9}$$

leaving the observed longitudinal relaxation rate independent of R_{1p} and the metal−nucleus distances. Normally, it is unknown a priori whether the fast- or the slow-exchange regime applies (*39*). However, in general, nuclei spatially close to the paramagnetic metal site will be in or close to the slow-exchange regime, while the more distant nuclei will be in the fast-exchange regime.

MATERIALS AND METHODS

Cloning, expression, and purification of the ^{15}N-labeled *E. coli* Trx were performed by the research group at Unizyme Laboratories, as described below.

Strains and Plasmids. E. coli strain BL21 (Novagen) was used as host for plasmid construction and for protein production. The Trx encoding sequence of the vector pTrx (Invitrogen) was amplified by PCR using two primers,

5-TTAAAAACATGTCCGATAAAATTATTCACCTGA-CTG and 5-GCCGAATTCGGATCCTTACTAGGCCAG-GTTAGCGTCG, thereby introducing flanking restriction sites, *Pci*I and *Bam*HI. The amplified 0.36 kb DNA fragment was digested by *Pci*I and *Bam*HI and ligated into the *Nco*I and *Bam*HI restriction sites of pTrcHisA (Invitrogen), resulting in the expression plasmid pCLU178-1.

Preparation and Purification of Trx. ^{15}N-Enriched Trx was produced by growing BL21 harboring pCLU178-1 in a totally defined medium, using $^{15}NH_4SO_4$ (>98% ^{15}N; Martek Biosciences Corp.) as the sole nitrogen source. The medium contained 2.5 g/L $^{15}NH_4SO_4$, 9 g/L KH_2PO_4, 6 g/L K_2HPO_4, 0.5 g/L sodium citrate, 1 g/L $MgSO_4$, 5 g/L glucose, 2 mg/L thiamin, 15 mg/L $CaCl_2$, 0.8 mg/L $FeCl_3$, and 100 mg/L ampicillin. Precultures of 5 mL were grown at 32 °C for 6 h in the ^{15}N-enriched medium. Each 5 mL preculture was transferred to 50 mL of medium in 250 mL shaker flasks, and incubation was continued overnight. Cultures of 450 mL in 2 L baffled shaker flasks were started by inoculation with overnight culture to $OD_{600} = 0.03-0.04$. Cultures were grown at 32 °C to mid-log phase, and expression of Trx was induced by adding isopropyl 1-thio-β-galactopyranoside (IPTG) to a final concentration of 0.06 mM. Cultures were grown for an additional 20 h at 32 °C, and cells were harvested by centrifugation and stored at −20 °C.

Frozen cell pellets from 900 mL of culture were thawed on ice in 65 mL of buffer A (25 mM Tris-HCl, pH 7.5, 0.3 M NaCl). Nuclease (Benzonase, 50 units/mL; Merck) was added, and the suspension was stirred for 30 min at 4−6 °C followed by homogenization (EmulsiFlex C5) at 150−200 MPa. Cell debris was removed by centrifugation for 45 min at 20000*g* and 4 °C, and the crude extract was collected (80 mL). Chromatographic steps were performed at 20−25 °C. The crude extract was desalted on a Sephadex G-25 F column (50 mm × 300 mm; Amersham Biosciences) equilibrated with buffer B (25 mM Tris-HCl, pH 8.0). The peak fraction was collected. The peak fraction was applied to a Q-Sepharose HP column (16 mm × 100 mm; Amersham Biosciences) equilibrated with buffer B (Tris-HCl, pH 8.0). Unbound material was washed out with 50 mL of buffer B. Trx was eluted using a linear gradient (450 mL) from buffer B to buffer C (25 mM Tris-HCl, pH 8.0, 0.15 M NaCl) at a flow rate of 1.5 mL/min. Elution fractions containing Trx were identified by SDS−PAGE analysis and pooled. The pooled fractions were saturated (20%) with solid ammonium sulfate, and the fractions were chromatographed on a phenyl-Sepharose 6 FF column (10 mm × 300 mm; Amersham Biosciences) equilibrated with buffer D (25 mM Tris-HCl, pH 8.0, 20% saturated with solid ammonium sulfate). Unbound material was removed by washing with 50 mL of buffer D. Trx was eluted in one step with 100% buffer B at a flow rate of 1.5 mL/min. The peak fraction was collected (15 mL) and loaded at a flow rate of 1 mL/min onto a Sephacryl S-100 HR column (26 mm × 900 mm; Amersham Biosciences). The column was equilibrated with buffer E (5 mM NaH_2PO_4, pH 7.0). Elution fractions containing Trx were identified by SDS−PAGE analysis and pooled.

NMR Samples. The purified protein was dissolved in 90% H_2O/10% D_2O with 50 mM sodium chloride. The protein concentration was 1.0 mM in all samples. The oxidized form of the protein was obtained by adding 5 μL of 50 mM H_2O_2 to each NMR sample (500 μL).

Samples with five different Ni^{2+} concentrations, 0.0, 0.1, 0.3, 0.5, and 1.0 mM, were prepared and used in the Ni^{2+} titration experiments. The pH was adjusted to 7.0 (meter reading) and the samples were sealed off under nitrogen. Coordination of the paramagnetic Ni^{2+} ion was achieved by adding the appropriate amounts of $NiCl_2 \cdot 6H_2O$. In the pH titration experiments the sample with 1.0 mM Ni^{2+} was used. NMR experiments were recorded for the pH values 7.0, 6.4, 5.7, 5.2, 4.7, 4.2, 3.7, and 3.2.

NMR Experiments. The NMR experiments were carried out at 298 K and a ^{1}H frequency of 500 and 800 MHz using Varian Unity Inova 500 and 800 spectrometers, the former being equipped with a cold probe. In all experiments, the ^{1}H carrier was placed on the HDO residual resonance at 4.774 ppm at 298 K. The ^{1}H−^{15}N HSQC spectra acquired at 500 MHz were collected with 4096 t_2 data points and 150 t_1 slices. The sweep widths were 10 and 2.2 kHz in the ^{1}H and ^{15}N dimension, respectively. The spectra acquired at 800 MHz were collected with 4096 t_2 data points and 200 t_1 slices. The sweep widths were 13 and 3.2 kHz in the ^{1}H and ^{15}N dimension, respectively.

The assignment of the ^{1}H−^{15}N HSQC spectra was performed on the basis of the previous assignments of the ^{1}H and ^{15}N nuclei of oxidized Trx at pH 5.7 and 308 K (*46*). The assignment of the HSQC spectra at other pH values was achieved by following the variation of the spectra with pH.

Measuring the Longitudinal Relaxation Rates. Information about the metal binding sites in Trx was obtained from the nonselective longitudinal relaxation rates of the amide protons in the protein as a function of both the paramagnetic metal ion concentration and the pH. The nonselective longitudinal relaxation rates of the amide protons were obtained from a series of two-dimensional, partially relaxed spectra acquired using the inversion recovery (IR) ^{1}H−^{15}N HSQC pulse sequence. The following IR relaxation delays (τ) were applied: 0.01, 0.02, 0.04, 0.08, 0.16, 0.32, 0.64, 1.2, 2.4, 4.8, and 8 s. The signal intensities were obtained by a least-squares fitting procedure that includes all of the partly relaxed spectra simultaneously, as described previously (*47*). The amide proton relaxation rates were obtained by a three-parameter single-exponential fit of the signal intensities, $M(\tau)$, versus the delay times, τ

$$M(\tau) = M^{eq} - (M^{eq} - M^0) \exp(-R_1\tau) \qquad (10)$$

Here, M^0 is the magnetization at time $\tau = 0$ s and M^{eq} is the equilibrium magnetization.

Impact of Fast Amide Proton Exchange on Magnetization Recoveries. For the majority of the amide protons in Trx, single-exponential relaxation recoveries were observed at pH 7.0. However, a minor part of the amide protons shows non-single-exponential relaxation recoveries. These amide protons are primarily located in loop regions and in the beginning of α-helical structures where the amide proton exchange is fast and, therefore, can obscure the relaxation recoveries, as pointed out previously (*48*, *49*). This is the case here as shown by the pH dependence of the relaxation recoveries. Thus, some of the amide protons have non-single-exponential relaxation recoveries at pH 7.0, whereas at lower pH values where the amide proton exchange rates are slower, the relaxation recoveries approach a single-exponential behavior.

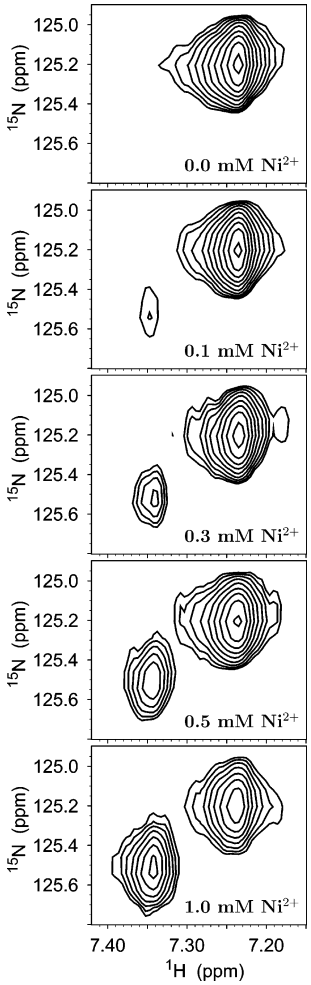

FIGURE 1: Excerpts of the 11.74 T ^{1}H−^{15}N HSQC spectra of Trx showing the ^{1}H−^{15}N resonance of residue A39 in the presence of Ni^{2+} at increasing concentrations and a constant pH of 7.0. The spectra reveal the appearance of an extra Ni^{2+}-dependent resonance of residue A39. The intensity of the extra signal increases with increasing Ni^{2+} concentration, indicating that the signal corresponds to a metal-bound form of the protein.

Therefore, reliable longitudinal relaxation rates at neutral pH can be obtained only for amide protons with slow-exchange rates. An extensive study of the amide proton exchange rates in both reduced and oxidized *E. coli* Trx was performed previously (*50*). Here, the results of this study were used to eliminate amide protons with relaxation rates that are affected by amide proton exchange.

Data Analysis. The least-squares analyses were carried out using an Apple Xserve G5 cluster with 34 processors using the program Funcfit.

RESULTS AND DISCUSSION

Ni^{2+} Titration. Upon addition of the paramagnetic Ni^{2+} ions, several new signals appear in the ^{1}H−^{15}N HSQC spectrum of Trx. The intensities of the new signals increase with increasing Ni^{2+} concentration. Furthermore, almost all of the new signals appear to be close to one of the signals in the metal-free sample and can easily be associated with one of these signals; i.e., some of the amide group signals split into two signals upon addition of Ni^{2+}. Figure 1 shows the two resonances of residue A39 for different Ni^{2+} concentrations. The appearance of the new signals and the observed variation of the signal intensities with the Ni^{2+} concentration clearly indicate that the two sets of signals correspond to a metal-free and a metal-bound form of the protein. Also, the chemical shifts of the two signals do not change when the Ni^{2+} concentration is increased, indicating that the amide group of A39 is in or close to the slow-exchange regime of the transverse relaxation.

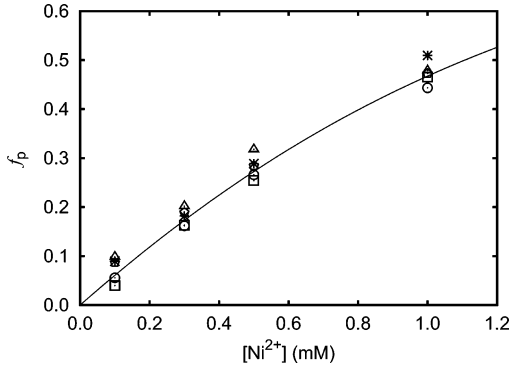

FIGURE 2: Fraction, f_p, of the metal-bound protein as a function of the total Ni^{2+} concentration. The fraction, f_p, was calculated from the intensities of the signals corresponding to the metal-free and the metal-bound form, respectively, using the double signals of residues A39 (○), T54 (□), V55 (*), A56 (⬠), and K57 (△) in the HSQC spectra recorded at 11.74 T. The solid line corresponds to an apparent dissociation constant, K_D^{app}, of 607 ± 26 μM, obtained by a least-squares fit, assuming that the metal ion binds to only one binding site in the protein.

Figure 2 shows the fraction, f_p, of the metal-bound protein as a function of the total Ni^{2+} concentration. The fractions were estimated from the intensities of the double signals of the amide groups of five residues, A39, T54, V55, A56, and K57, all with well-resolved signals in the HSQC spectra. For each of the applied Ni^{2+} concentrations, the five f_p ratios are almost identical. The variation of the ratios with increasing Ni^{2+} concentration gives an apparent dissociation constant, $K_D^{app} = 607 \pm 26\ \mu$M, assuming that the metal ion binds to only one binding site. The solid line in Figure 2 corresponds to this dissociation constant.

The longitudinal relaxation rates of the amide protons were measured at 11.74 and 18.79 T for each of the applied Ni^{2+} concentrations. For amide protons with separate signals of the metal-free and the metal-bound forms, the rate of the metal-free signal was measured. The increase in the relaxation rates upon addition of the paramagnetic metal ion varies considerably among the different amide protons. In particular, the relaxation rates of the amide protons spatially close to the N-terminal end of the protein are enhanced considerably, which shows that the Ni^{2+} ions interact specifically with a binding site near the N-terminal end of the protein. The precise location of this site was determined by the quantitative least-squares analysis described below.

However, also amide protons spatially close to D20 have significantly enhanced relaxation rates, even though this residue is located about 20 Å from the N-terminus. This shows that the metal ion binds also to the side chain carboxylate group of D20. Similarly, a series of other amide protons spatially close to carboxylate groups have relaxation enhancements that cannot be ascribed to the metal ion at the N-terminus only. This multiple interaction with Ni^{2+} results in a rather complicated pattern of relaxation rates that requires more experimental information and a simultaneous

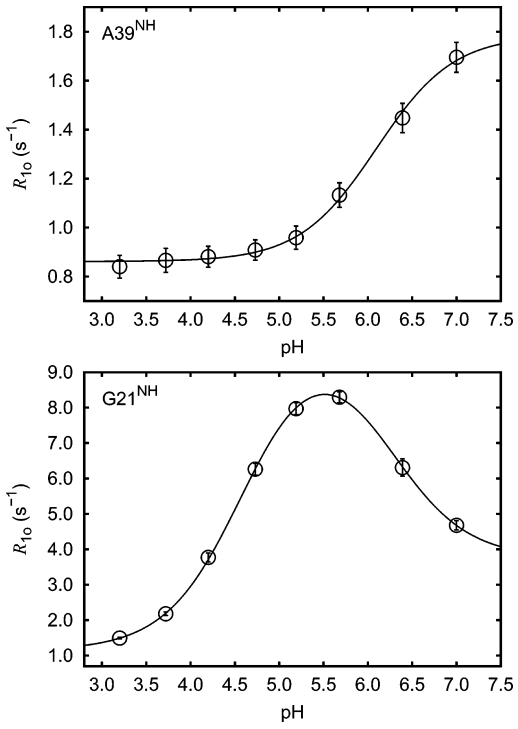

FIGURE 3: pH titration curves for the amide protons $A39^{NH}$ (upper panel) and $G21^{NH}$ (lower panel). A sample of 1.0 mM Trx and 1.0 mM Ni^{2+} containing 50 mM NaCl was used. The observed longitudinal relaxation rates were measured at 11.74 T for eight different pH values in the range from 3.2 to 7.0. The relaxation rate of the amide proton $A39^{NH}$ follows a single-step titration (solid line, upper panel) with a pK_a value of 6.10 ± 0.05. The relaxation rate of the amide proton $G21^{NH}$ follows a two-step titration (solid line, lower panel) with pK_a values of 4.60 ± 0.01 and 6.23 ± 0.05. The curvature of the pH dependences shows that $A39^{NH}$ is affected by only one Ni^{2+} binding site, while $G21^{NH}$ is affected by two or more metal binding sites.

analysis of all the relaxation rates to unravel the relaxation pattern and to identify and characterize the individual binding sites. Therefore, the pH dependence of the relaxation rates at constant Ni^{2+} and protein concentration (1.0 mM) was obtained at 11.74 T and included in the least-squares analysis of the entire data set, as described below.

pH Titration. Qualitatively, the intensity of the extra signals that are observed for some of the amide groups in the presence of Ni^{2+} at pH 7.0 (see Figure 1) decreases with decreasing pH and disappears below pH 5.5. Thus, a pH dependence of the Ni^{2+} binding is clearly observed for the residues with an extra signal corresponding to the metal-bound form. For the carboxylate binding sites, where only a single exchange-averaged signal of the metal-free and metal-bound form is observed, the pH dependence of the Ni^{2+} binding can be monitored through the pH dependence of the relaxation rates. Therefore, the longitudinal relaxation rates of the amide protons were measured at 11.74 T for each pH value and a Ni^{2+} concentration of 1.0 mM. This is illustrated in Figure 3 for the relaxation rate of the amide proton $A39^{NH}$ (upper panel). The relaxation rate of this proton follows a single-step titration with a pK_a value of 6.10 ± 0.05, reflecting the pH dependence of the Ni^{2+} binding. At pH 7.0 the metal ion binds to the protein as shown by the enhanced relaxation rate. However, with decreasing pH the metal coordinating group becomes protonated, and the metal ion is released from the binding site, that is

$$TrxNi^{2+} + H^+ \rightleftharpoons TrxH^+ + Ni^{2+} \quad (11)$$

Similar single-step pH titration curves were obtained for 16 other amide protons. The pK_a values obtained from the titration curves of these protons are almost identical within experimental errors with a weighted average value of 6.00 ± 0.03. The simple, single-step pH titration curves show that these amide protons are affected by only one metal binding site, while the identical pK_a values indicate that they are affected by the same metal binding. Moreover, the size of the obtained apparent pK_a value ($pK_a^{app} = 6.00$) indicates that the metal ion is coordinated to the free N-terminal NH_2 group of residue S1.

For a series of amide protons, the pH dependence of the relaxation rates is more complex and does not correspond to a single-step titration, as illustrated in Figure 3 for the relaxation rate of $G21^{NH}$ (lower panel). This rate follows a two-step titration curve with pK_a values of 6.23 ± 0.05 and 4.60 ± 0.01. Therefore, $G21^{NH}$ is affected by Ni^{2+} bound to two different binding sites with different binding characteristics. As the pH is lowered from neutral pH, the binding site with the highest pK_a value ($pK_a = 6.23$) becomes protonated and the Ni^{2+} ions will be released. Thus, more Ni^{2+} ions become available to the binding site with the lower pK_a value ($pK_a = 4.60$). Consequently, the relaxation rate increases when the pH is lowered from 7.0 to 5.5. Below pH 5.5, also the binding site with the lower pK_a value gets protonated and the relaxation rate decreases. The obtained pK_a value of 6.23 is close to the value obtained from the single-step titration curves, while the value of 4.60 is close to the pK_a value expected for a side chain carboxylate group.

Other amide protons are also affected by more than one metal binding site, although not reflected in the titration curves as clearly as in the case of $G21^{NH}$. Therefore, to unravel the pattern of relaxation rates and to identify and characterize the individual binding sites, a simultaneous and quantitative analysis of all the experimental relaxation rates is necessary.

Quantitative Analysis of Relaxation Rates. Initially, the location of the binding site that gives rise to the double signals in the HSQC spectra of the metal-containing protein was determined by a least-squares analysis. This analysis involved only the 16 amide protons with single-step pH titration curves and the average pK_a value of 6.00 (see Figure 3, upper panel). As mentioned above, these amide protons are affected by only one metal binding site characterized by the fraction of the metal-bound protein (see Figure 2) and the rate of exchange, k, between the metal-free and the metal-bound form of the protein. The relaxation rates of these amide protons are described by eq 3. On the basis of the structure of the protein [the oxidized form of Trx; PDB 1XOA (*51*)] and the dependence of the observed relaxation rates on the Ni^{2+} concentration, a series of parameters were determined by a least-squares fit of eqs 3−7 to the observed longitudinal relaxation rates. The parameters include the position of the Ni^{2+} ion at the binding site, the corresponding first-order rate constant, k_{off}, and the diamagnetic contribution, R_{1d}, to the relaxation rate of each of the 16 amide protons. The electron relaxation rate, $R_{1e} = 7.6 \times 10^9\ s^{-1}$, found previously for Ni^{2+} in its complex with HHP-tagged Trx (*44*) was used in the analysis. This rate is in agreement with the field dependence of the paramagnetic relaxation enhancements of

the amide protons observed here between 11.74 and 18.79 T. Also, a rotational correlation time of 6.16 ns was used (*30*), although it has little or no impact on the analysis since the correlation time $\tau_{c,1}$ is completely dominated by R_{1e} (see eq 6). Furthermore, the second term in eq 5, which involves the electron Larmor frequency, can be neglected due to the size of the transverse electron relaxation rate, R_{2e} (*44*).

The least-squares analysis shows that the Ni^{2+} ion is located near the N-terminal end of the protein in close proximity to the N-terminal NH_2 group of S1 and the side chain carboxylate group of D2. Previously, the X-ray structure was obtained of *E. coli* Trx crystallized in the presence of cupric acetate (*52*). The structure reveals two cupric ions bound to the protein in the asymmetric unit. Each one of the cupric ions is six-coordinated in a distorted octahedral geometry with the cupric ions bound to the amino-terminal nitrogen atom, the amide nitrogen of residue D2, and the side chain atom OD1 of residue D2 in one molecule. In a symmetry-related molecule, the cupric ions are coordinated to both side chain oxygen atoms of residue D10. Also, each one of the cupric ions is coordinated to a water molecule. The results of the analysis here show that Ni^{2+} binds to the N-terminal binding site of Trx in solution in a similar manner. This is illustrated in Figure 4, which shows a superposition of the backbone (residues 5−108) of the solution structure (red trace) and the X-ray structure (gray trace) of Trx.

Subsequently, also the pH-dependent relaxation rates at 11.74 T were included in the analysis. Thus, the total number of binding sites and their location, together with the binding characteristics of the sites, were determined by a simultaneous, least-squares analysis of all the relaxation rates obtained as a function of the Ni^{2+} concentration and the pH. In the case of multiple metal binding sites, the observed nuclear relaxation rate, R_{1o}, is given by

$$R_{1o} = \frac{2R_{1d} + R_{1p} + k}{2} - \sqrt{\left(\frac{R_{1p} + k}{2}\right)^2 - kf_pR_{1p}} + \sum_i^N f_{p,i}R_{1p,i} \quad (12)$$

Here, $N + 1$ is the number of metal binding sites, $f_{p,i}$ is the occupancy of the ith binding site, and $R_{1p,i}$ is the paramagnetic relaxation enhancement of the nucleus caused by the metal ion in the ith binding site. Thus, it is assumed that each amide proton in Trx is in the intermediate-exchange regime with respect to one binding site, i.e., the N-terminal binding site, as indicated by the observation of the double signals, and in the fast-exchange regime with respect to N other binding sites, i.e., the carboxylate binding sites. The latter assumption is supported by the available information on the binding modes of Ni^{2+} to proteins and peptides, which indicate that the carboxyl groups of aspartate and glutamate residues only play a secondary role for Ni^{2+} binding sites, the imidazole groups of histidine residues and the thiol groups of cysteine residues being the preferred donor groups for Ni^{2+} binding (*53*).

Since the occupancy of the N-terminal binding site was determined independently in the Ni^{2+} titration (see above and Figure 2), it was included as a fixed parameter in the analysis. Thus, at pH 7.0 and equivalent amounts of Trx and Ni^{2+} (1.0 mM), the fraction, f_p, of the N-terminal metal-bound protein is 0.47 (see Figure 2). From this value and the apparent pK_a^{app} value (6.00) of the N-terminal binding site, the fraction, f_p, of N-terminal metal-bound protein was calculated for each of the pH values in the pH titration experiments and included as fixed parameters in the least-squares analysis.

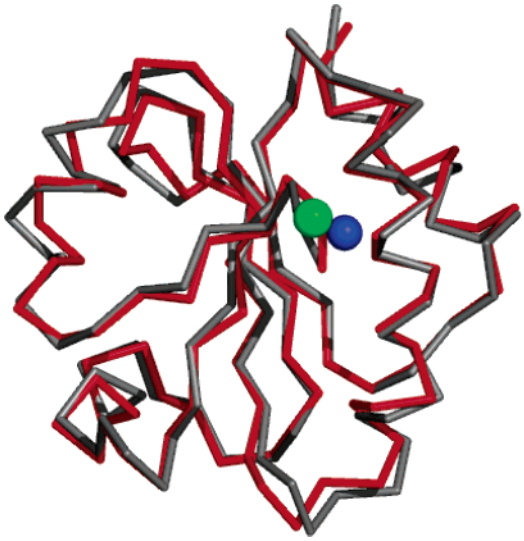

FIGURE 4: Superposition of the backbone (residues 5−108) of the solution structure (*57*) (red trace) and the X-ray structure (*52*) (gray trace) of *E. coli* Trx. The blue sphere is the Cu^{2+} ion located in the X-ray structure of Trx, while the green sphere is the Ni^{2+} ion bound to the protein in solution. The two metal ions are spatially close, indicating that the Ni^{2+} ion in solution coordinates to the same atoms in Trx as the Cu^{2+} ion in the crystal phase. The figure was prepared with the program PyMOL (*58*).

In contrast, the occupancies of the carboxylate binding sites must be determined in the total least-squares analysis. Therefore, two simultaneous equilibria were considered for each carboxylate binding site, B_i, in Trx

$$B_i + Ni^{2+} \rightleftharpoons B_iNi^{2+} \quad (13)$$

$$B_i + H^+ \rightleftharpoons B_iH^+ \quad (14)$$

By including these equilibria in the analysis, the dissociation constant, K_D, for the Ni^{2+} binding and the pK_a value can be determined through eq 12 for each of the metal coordinating groups.

It should be noted that the relaxation rates of several affected amide protons must be available for each carboxylate binding site to obtain a reliable characterization of the sites. This condition was not fulfilled for one of the carboxylate binding sites (E85, see below), where some of the relaxation rates could not be determined either because of spectral overlap or because of fast amide proton exchange at pH 7.0. Therefore, reasonable values of pK_a and K_D were chosen for this site in the least-squares analysis. Thus, the pK_a value for the E85 binding site was fixed at 4.60 on the basis of the pH titration curve for the amide proton $G84^{NH}$. This amide proton titrates with two apparent pK_a values, 6.24 ± 0.09 and 4.60 ± 0.03, according to the pH dependence of its relaxation rate. The former value corresponds to the titration of the N-terminal binding site and the latter to the

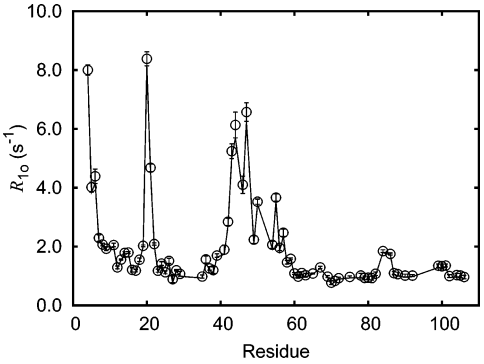

FIGURE 5: Per-residue comparison of the experimental longitudinal relaxation rates (○) obtained at 11.74 T, and the rates (full drawn line) calculated on the basis of the structure of Trx and the positions of the Ni^{2+} ions as obtained in the least-squares analysis (see Figure 7) using eq 12. The experimental longitudinal relaxation rates were obtained from a 1.0 mM sample of Trx at pH 7.0 containing 1.0 mM Ni^{2+}.

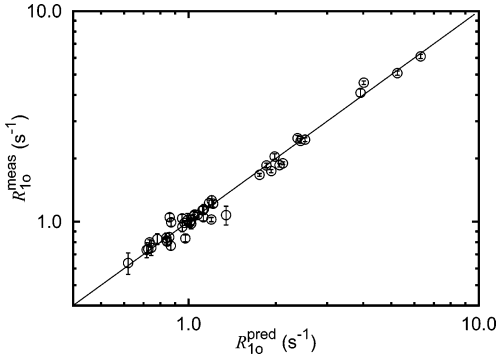

FIGURE 6: Comparison of the relaxation rates R_{1o}^{pred} and R_{1o}^{meas}. The R_{1o}^{pred} rates were calculated using the parameters obtained in the least-squares fit by omitting 5% of the measured relaxation rates, R_{1o}^{meas}. The data omitted in the analysis were randomly selected and contain relaxation rates obtained at different pH values and different Ni^{2+} concentrations.

titration of the E85 carboxylate group. Since the occupancy of the carboxylate binding site is small (K_D is large), the pH dependence of $[B_iNi^{2+}]$ will be controlled by the pK_a value of B_iH^+, while it, in practice, is unaffected by the K_D value. For a pK_a value of 4.60, the best agreement with the experimental data was obtained for a dissociation constant, K_D, of 20 mM for the E85 binding site.

A total of 856 relaxation rates distributed among 88 different amide protons were included in the least-squares fit. The number of variables was 112, including 4 parameters for the N-terminal binding site, 5 parameters for each of the carboxylate binding sites, and 88 R_{1d} values, one for each of the included amide protons. It should be emphasized that the pH titration data are essential for the convergence of the least-squares fit and, in general, for the quality of the analysis presented here. Not only do the pH titration experiments allow a distinction between the amide protons affected only by the N-terminal binding site and those affected by several binding sites, the pH titration experiments also provide the information necessary for determining the occupancies of the different carboxylate binding sites. Last, but not least, the pH titration experiments provide reliable relaxation rates at low pH in the cases where the rates at neutral pH are affected by fast amide proton exchange that obscure the information about the Ni^{2+}−amide proton interactions (*48*, *49*).

The quality of the least-squares analysis was primarily evaluated by comparing the experimental longitudinal relaxation rates of the amide protons with those calculated from the parameters obtained in the least-squares analysis (see below). Figure 5 shows a per-residue comparison of the two sets of rates. In general, the agreement between the experimental and the calculated relaxation rates is good. Thus, almost all of the calculated relaxation rates are within the error bars of the experimental rates. A similar agreement between the experimental and the calculated rates is found for the other Ni^{2+} concentrations and pH values.

A further evaluation of the quality of the fit was made by omitting a small portion (5%, i.e., 45 relaxation rates) of the relaxation data and back-calculating the data from the subsequent fit. The 45 relaxation rates were randomly selected among the 856 observables and include relaxation rates at different pH values and different Ni^{2+} concentrations.

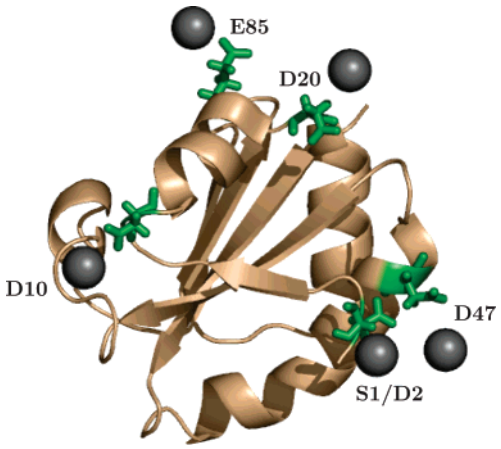

FIGURE 7: Structure of Trx showing the five different Ni^{2+} binding sites. The carboxylate side chains are shown in green while the Ni^{2+} ions are shown in gray. The figure was prepared with the program PyMOL (*58*).

The quality was evaluated through the *Q*-parameter defined as (*54*)

$$Q = \mathrm{rms}(R_{1o}^{meas} - R_{1o}^{pred})/\mathrm{rms}(R_{1o}^{meas}) \qquad (15)$$

Here, R_{1o}^{meas} are the measured relaxation rates, which were omitted in the least-squares analysis, and R_{1o}^{pred} are the relaxation rates predicted from the parameters obtained in the least-squares fit. Six least-squares analyses were performed each time omitting 45 randomly selected relaxation rates. The average *Q*-parameter obtained from these calculations was 16 ± 2%. Figure 6 shows a comparison of the measured and the predicted relaxation rates from one of these analyses.

Charaterization of Metal Binding Sites. Qualitatively, the total least-squares fit shows that Ni^{2+} binds specifically and with an appreciable affinity to only four side chain carboxylate groups, in addition to the N-terminal binding site. In the least-squares analysis, the number of carboxylate binding sites was found by increasing the number of binding sites until a satisfactory agreement with the experimental data was obtained. The four carboxylate groups are those of residues D10, D20, D47, and E85, while the N-terminal binding site includes the N-terminal NH_2 group of S1 and the side chain carboxylate group of D2. Figure 7 shows the

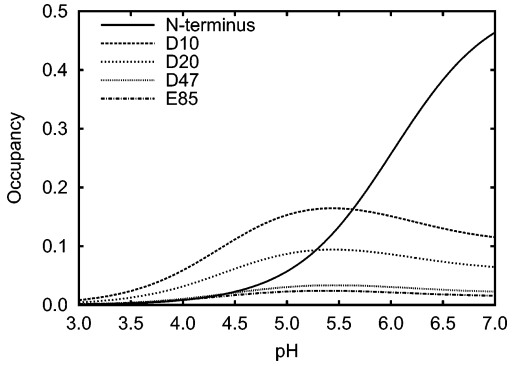

FIGURE 8: pH dependence of the occupancies of the five metal binding sites in Trx. The occupancies were calculated using the dissociation constants and pK_a values obtained in the least-squares analysis (see text).

structure of Trx with the side chains of D2, D10, D20, D47, and E85 in green and the bound Ni^{2+} ions in gray. As it appears from the figure, the Ni^{2+} ions are located in close proximity to the side chain carboxylate groups, although the distances of some of the metal ions from the carboxylate groups are slightly larger than expected. It should be noted, however, that the structure shown here is the unmodified metal-free solution structure, while in the actual metal-bound structure some of the side chains most likely are rearranged slightly in order to coordinate to the metal ion.

Quantitatively, the following dissociation constants, K_D, were obtained for the individual carboxylate binding sites: D10 ($K_D = 2.4 \pm 0.7$ mM), D20 ($K_D = 4.6 \pm 1.2$ mM), and D47 ($K_D = 13.6 \pm 4.8$ mM). Furthermore, the following pK_a values were obtained for the carboxylate metal binding sites: D10 (4.6 ± 0.1), D20 (4.7 ± 0.1), and D47 (4.7 ± 0.1). Finally, for the N-terminal binding site a rate constant $k_{off} = 7.0 \pm 0.3\ s^{-1}$ was obtained in the least-squares analysis.

Using the K_D and pK_a values obtained in the least-squares fit and the fixed parameters of the E85 binding site, the pH dependence of the occupancies of the binding sites in Trx was calculated for a constant Ni^{2+} and protein concentration (1.0 mM). The results are shown in Figure 8. It is seen that, for equivalent amounts of the protein and Ni^{2+}, the occupancies at pH 7.0 are S1/D2 (47%), D10 (11%), D20 (7%), D47 (3%), and E85 (2%), respectively, leaving 30% of the Ni^{2+} ions unbound at these experimental conditions.

From the occupancy of 47% at pH 7.0 of the N-terminal binding site, and its pH dependence that follows a titration curve with an apparent pK_a value of 6.0 (see above), a K_D value of 235 μM and a pK_a value of 6.65 were estimated. This pK_a value is somewhat lower than the value of 7.32 ± 0.05 obtained previously for the N-terminal amino group, using the pH-induced chemical shift changes of the α- and β-protons of residue S1 (*55*). Most likely, the lower pK_a value obtained here corresponds to an average pK_a value of the N-terminal amino group of residue S1 and the side chain carboxylate group of residue D2. This suggestion is supported by the fact that both functional groups are potential Ni^{2+} binding groups and that the Ni^{2+} ion is located close to the two groups, according to the analysis here.

It is interesting to compare the K_D values obtained for the different carboxylate binding sites. Thus, although the K_D value of D10 is smaller than that of D20, i.e., D10 binds Ni^{2+} more tightly than D20, the relaxation rates of the amide protons close to D20 are significantly more enhanced than the amide protons close to D10 (see Figure 5). However, residues D9 and D13 also have side chain carboxylate groups. Therefore, the K_D value obtained for D10 may be affected by interactions between Ni^{2+} and residues D9 and D13. This leads to a larger occupancy of the D10 binding site while at the same time the distance from the side chain carboxylate group of D10 to the metal ion is longer than in the case of D20.

Table 1: Solvent Accessibility (%) of the Aspartic and Glutamic Acid Residues in *E. coli* Trx[a]

residue	solvent accessibility (%)	residue	solvent accessibility (%)
D2	21.4	D43	10.9
D9	16.5	E44	25.8
D10	47.5	D47	24.2
D13	21.8	E48	26.3
D15	19.1	D61	24.4
D20	56.0	E85	43.5
D26	0.0	E101	42.2
E30	42.0	D104	28.6

[a] Calculated using MOLMOL (*56*) and a probe size of 1.4 Å.

Finally, the metal binding capability of the side chain carboxylate groups in Trx was compared with the solvent accessibility of the residues, as shown in Table 1. The solvent accessibility was calculated for each residue using the program MOLMOL (*56*) and a probe size of 1.4 Å. As it appears from the table, D10, D20, and E85 have the highest solvent accessibilities. Therefore, these residues are more likely to interact with the Ni^{2+} ions than the remaining residues with side chain carboxylate groups, in agreement with their metal binding capability found here. Also, the metal ions are more likely to interact with carboxylate groups that cluster close together on the protein surface (*23*). This might be the case for the D47 binding site, which is surrounded by the aspartic and glutamic acids D43, E44, and E48.

CONCLUSION

The detailed analysis presented here demonstrates that potential metal binding sites in proteins can be identified and characterized using paramagnetic NMR relaxation. Thus, for each binding site in the model protein *E. coli* thioredoxin, the occupancy and the pK_a value of the metal binding site were determined by a least-squares analysis of the longitudinal relaxation rates of the amide protons using the structure of the protein. Although the approach is computationally intensive, it is conceptually simple, and in general it should be applicable in studies of proteins, where interactions with metal ions are necessary for the function. Because of the sensitivity of the method it should be applicable even in cases where the metal−protein interactions are relatively weak.

ACKNOWLEDGMENT

We thank D. Flemming Hansen, Søren M. Kristensen, Henrik Gesmar, Mathias A. S. Hass, and Kim R. Hejnæs for helpful discussions and Else Philipp, Jens Duus, and Bent O. Petersen for technical assistance. The 800 MHz spectra were acquired at the Danish Instrument Center for NMR Spectroscopy of Biological Macromolecules.

REFERENCES

1. Yocom, K. M., Shelton, J. B., Shelton, J. R., Schroeder, W. A., Worosila, G., Isied, S. S., Bordignon, E., and Gray, H. B. (1982)

Preparation and Characterization of a Pentaammineruthenium(III) Derivative of Horse Heart Ferricytochrome *c*, *Proc. Natl. Acad. Sci. U.S.A. 79*, 7052−7055.
2. Yamashita, M. M., Wesson, L., Eisenman, G., and Eisenberg, D. (1990) Where Metal Ions Bind in Proteins, *Proc. Natl. Acad. Sci. U.S.A. 87*, 5648−5652.
3. Vallee, B. L., and Auld, D. S. (1990) Active-Site Zinc Ligands and Activated H_2O of Zinc Enzymes, *Proc. Natl. Acad. Sci. U.S.A. 87*, 220−224.
4. Vallee, B. L., Coleman, J. E., and Auld, D. S. (1991) Zinc Fingers, Zinc Clusters, and Zinc Twists in DNA-Binding Protein Domains, *Proc. Natl. Acad. Sci. U.S.A. 88*, 999−1003.
5. Cunningham, B. C., Mulkerrin, M. G., and Wells, J. A. (1991) Dimerization of Human Growth Hormone by Zinc, *Science 253*, 545−548.
6. Higaki, J. N., Fletterick, R. J., and Craik, C. S. (1992) Engineered Metalloregulation in Enzymes, *Trends Biochem. Sci. 17*, 100−104.
7. Gregory, D. S., Martin, A. C. R., Cheetham, J. C., and Rees, A. R. (1993) The Prediction and Characterization of Metal Binding Sites in Proteins, *Protein Eng. 6*, 29−35.
8. Nayal, M., and Cera, E. D. (1994) Predicting Ca^{2+}-Binding Sites in Proteins, *Proc. Natl. Acad. Sci. U.S.A. 91*, 817−821.
9. Jackson, G. S., Murray, I., Hosszu, L. L. P., Gibbs, N., Waltho, J. P., Clarke, A. R., and Collinge, J. (2001) Location and Properties of Metal-Binding Sites on the Human Prion Protein, *Proc. Natl. Acad. Sci. U.S.A. 98*, 8531−8535.
10. Yang, W., Lee, H.-W., Hellinga, H., and Yang, J. J. (2002) Structural Analysis, Identification, and Design of Calcium-Binding Sites in Proteins, *Proteins: Struct., Funct., Genet. 47*, 344−356.
11. Glusker, J. P. (1991) Structural Aspects of Metal Liganding to Functional Groups in Proteins, *Adv. Protein Chem. 42*, 1−76.
12. Regan, L. (1993) The Design of Metal-Binding Sites in Proteins, *Annu. Rev. Biophys. Biomol. Struct. 22*, 257−281.
13. Jernigan, R., Raghunathan, G., and Bahar, I. (1994) Characterization of Interactions and Metal Ion Binding Sites in Proteins, *Curr. Opin. Struct. Biol. 4*, 256−263.
14. Lu, Y., and Valentine, J. S. (1997) Engineering Metal-Binding Sites in Proteins, *Curr. Opin. Struct. Biol. 7*, 495−500.
15. Lu, Y., Berry, S. M., and Pfister, T. D. (2001) Engineering Novel Metalloproteins: Design of Metal-Binding Sites into Native Protein Scaffolds, *Chem. Rev. 101*, 3047−3080.
16. Dudev, T., and Lim, C. (2003) Principles Governing Mg, Ca, and Zn Binding and Selectivity in Proteins, *Chem. Rev. 103*, 773−787.
17. McDonald, C. C., and Phillips, W. D. (1969) Perturbation of the PMR Spectrum of Lysozyme by Co^{2+}, *Biochem. Biophys. Res. Commun. 35*, 43−51.
18. Reuben, J. (1971) Gadolinium(III) as Paramagnetic Probe for Proton Relaxation Studies of Biological Macromolecules. Binding to Bovine Serum Albumin, *Biochemistry 10*, 2834−2838.
19. Agresti, D. G., Lenkinski, R. E., and Glickson, J. D. (1977) Lanthanide Induced NMR Perturbations of Hew Lysozyme: Evidence for Nonaxial Symmetry, *Biochem. Biophys. Res. Commun. 76*, 711−719.
20. Lane, A. N., and Jardetzky, O. (1985) Identification of Surface Residues in the trp Repressor of *Escherichia coli*, *Eur. J. Biochem. 152*, 411−418.
21. Schmiedeskamp, M., and Klevit, R. E. (1997) Paramagnetic Cobalt as a Probe of the Orientation of an Accessory DNA-Binding Region of the Yeast ADR1 Zinc-Finger Protein, *Biochemistry 36*, 14003−14011.
22. Liepinsh, E., Baryshev, M., Shapiro, A., Ingelman-Sundberg, M., Otting, G., and Mkrtchian, S. (2001) Thioredoxin Fold as Homodimerization Module in the Putative Chaperone ERp29: NMR Structures of the Domains and Experimental Model of the 51 kDa Dimer, *Structure 9*, 457−471.
23. Aime, S., D'Amelio, N., Fragai, M., Lee, Y.-M., Luchinat, C., Terreno, E., and Valensin, G. (2002) A Paramagnetic Probe to Localize Residues Next to Carboxylates on Protein Surfaces, *J. Biol. Inorg. Chem. 7*, 617−622.
24. Bertini, I., Couture, M. M. J., Donaire, A., Eltis, L. D., Felli, I. C., Luchinat, C., Piccioli, M., and Rosato, A. (1996) The Solution Structure Refinement of the Paramagnetic Reduced High-Potential Iron−Sulfur Protein I From *Ectothiorhodospira halophila* by Using Stable Isotope Labeling and Nuclear Relaxation, *Eur. J. Biochem. 241*, 440−452.
25. Gaponenko, V., Dvoretsky, A., Walsby, C., Hoffman, B. M., and Rosevear, P. R. (2000) Calculation of *z*-Coordinates and Orientational Restraints Using a Metal Binding Tag, *Biochemistry 39*, 15217−15224.
26. Donaldson, L. W., Skrynnikov, N. R., Choy, W.-Y., Muhandiram, D. R., Sarkar, B., Forman-Kay, J. D., and Kay, L. E. (2001) Structural Characterization of Proteins with an Attached ATCUN Motif by Paramagnetic Relaxation Enhancement NMR Spectroscopy, *J. Am. Chem. Soc. 123*, 9843−9847.
27. Mal, T. K., Ikura, M., and Kay, L. E. (2002) The ATCUN Domain as a Probe of Intermolecular Interactions: Application to Calmodulin-Peptide Complexes, *J. Am. Chem. Soc. 124*, 14002−14003.
28. Gaponenko, V., Altieri, A. S., Li, J., and Byrd, R. A. (2002) Breaking Symmetry in the Structure Determination of (Large) Symmetric Protein Dimers, *J. Biomol. NMR 24*, 143−148.
29. Gaponenko, V., Sarma, S. P., Altieri, A. S., Horita, D. A., Li, J., and Byrd, R. A. (2004) Improving the Accuracy of NMR Structures of Large Proteins Using Pseudocontact Shifts as Long-Range Restraints, *J. Biomol. NMR 28*, 205−212.
30. Jensen, M. R., Lauritzen, C., Dahl, S. W., Pedersen, J., and Led, J. J. (2004) Binding Ability of a HHP−Tagged Protein Towards Ni^{2+} Studied by Paramagnetic NMR Relaxation: The Possibility of Obtaining Long-Range Structure Information, *J. Biomol. NMR 29*, 175−185.
31. Nomura, M., Kobayashi, T., Kohno, T., Fujiwara, K., Tenno, T., Shirakawa, M., Ishizaki, I., Yamamoto, K., Matsuyama, T., Mishima, M., and Kojima, C. (2004) Paramagnetic NMR Study of Cu^{2+}-IDA Complex Localization on Protein Surface and its Application to Elucidate Long Distance Information, *FEBS Lett. 566*, 157−161.
32. Petros, A. M., Mueller, L., and Kopple, K. D. (1990) NMR Identification of Protein Surfaces Using Paramagnetic Probes, *Biochemistry 29*, 10041−10048.
33. Scarselli, M., Bernini, A., Segoni, C., Molinari, H., Esposito, G., Lesk, A. M., Laschi, F., Temussi, P., and Niccolai, N. (1999) Tendamistat Surface Accessibility to the TEMPOL Paramagnetic Probe, *J. Biomol. NMR 15*, 125−133.
34. Battiste, J. L., and Wagner, G. (2000) Utilization of Site-Directed Spin Labeling and High-Resolution Heteronuclear Nuclear Magnetic Resonance for Global Fold Determination of Large Proteins with Limited Nuclear Overhauser Effect Data, *Biochemistry 39*, 5355−5365.
35. Gaponenko, V., Howarth, J. W., Columbus, L., Gasmi-Seabrook, G., Yuan, J., Hubbell, W. L., and Rosevear, P. R. (2000) Protein Global Fold Determination Using Site-Directed Spin and Isotope Labeling, *Protein Sci. 9*, 302−309.
36. Holmgren, A. (1985) Thioredoxin, *Annu. Rev. Biochem. 54*, 237−271.
37. McConnell, H. M. (1958) Reaction Rates by Nuclear Magnetic Resonance, *J. Chem. Phys. 28*, 430−431.
38. Ma, L., Jørgensen, A.-M. M., Sørensen, G. O., Ulstrup, J., and Led, J. J. (2000) Elucidation of the Paramagnetic R_1 Relaxation of Heteronuclei and Protons in Cu(II) Plastocyanin from *Anabaena variabilis*, *J. Am. Chem. Soc. 122*, 9473−9485.
39. Jensen, M. R., Hansen, D. F., and Led, J. J. (2002) A General Method for Determining the Electron Self-Exchange Rates of Blue Copper Proteins by Longitudinal NMR Relaxation, *J. Am. Chem. Soc. 124*, 4093−4096.
40. Solomon, I. (1955) Relaxation Processes in a System of Two Spins, *Phys. Rev. 99*, 559−565.
41. Donaire, A., Salgado, J., and Moratal, J.-M. (1998) Determination of the Magnetic Axes of Cobalt(II) and Nickel(II) Azurins from ^{1}H NMR Data: Influence of the Metal and Axial Ligands on the Origin of Magnetic Anisotropy in Blue Copper Proteins, *Biochemistry 37*, 8659−8673.
42. Bertini, I., Briganti, F., and Luchinat, C. (1985) The Electron-Nucleus Dipolar Coupling in Slow Rotating Systems. 2. The Effect of g Anisotropy and Hyperfine Coupling When $S = 1/2$ and $I = 1/2$, *J. Magn. Reson. 63*, 41−55.
43. Bertini, I., Luchinat, C., and Vasavada, K. V. (1990) The Effect of Magnetic Anisotropy on the Longitudinal Nuclear Relaxation Time in Paramagnetic Systems, *J. Magn. Reson. 89*, 243−254.
44. Jensen, M. R., and Led, J. J. (2004) Determination of the Electron Relaxation Rates in Paramagnetic Metal Complexes: Applicability of Available NMR Methods, *J. Magn. Reson. 167*, 169−177.
45. Sharp, R. R. (1993) Effect of Zero Field Splitting Interactions on the Paramagnetic Relaxation Enhancement of Nuclear Spin Relaxation Rates in Solution, *J. Chem. Phys. 98*, 912−921.

46. Chandrasekhar, K., Krause, G., Holmgren, A., and Dyson, H. J. (1991) Assignment of the ^{15}N NMR Spectra of Reduced and Oxidized *Escherichia coli* Thioredoxin, *FEBS Lett. 284*, 178−183.
47. Hansen, D. F., and Led, J. J. (2004) Mapping the Electronic Structure of the Blue Copper Site in Plastocyanin by NMR Relaxation, *J. Am. Chem. Soc. 126*, 1247−1252.
48. Gryk, M. R., Finucane, M. D., Zheng, Z., and Jardetzky, O. (1995) Solution Dynamics of the *trp* Repressor: A Study of Amide Proton Exchange by T_1 Relaxation, *J. Mol. Biol. 246*, 618−627.
49. Zheng, Z., Gryk, M. R., Finucane, M. D., and Jardetzky, O. (1995) Investigation of Protein Amide-Proton Exchange by ^{1}H Longitudinal Spin Relaxation, *J. Magn. Reson., Ser. B 108*, 220−234.
50. Jeng, M.-F., and Dyson, H. J. (1995) Comparison of the Hydrogen-Exchange Behavior of Reduced and Oxidized *Escherichia coli* Thioredoxin, *Biochemistry 34*, 611−619.
51. Berman, H. M., Westbrook, J., Feng, Z., Gilliland, G., Bhat, T. N., Weissig, H., Shindyalov, I. N., and Bourne, P. E. (2000) The Protein Data Bank, *Nucleic Acids Res. 28*, 235−242.
52. Katti, S. K., LeMaster, D. M., and Eklund, H. (1990) Crystal Structure of Thioredoxin from *Escherichia coli* at 1.68 Å Resolution, *J. Mol. Biol. 212*, 167−184.
53. Zoroddu, M. A., Peana, M., and Kowalik-Jankowska, T. (2002) The Binding of Ni(II) and Cu(II) with the N-terminal Tail of the Histone H4, *J. Chem. Soc., Dalton Trans.*, 458−465.
54. Cornilescu, G., Marquardt, J. L., Ottiger, M., and Bax, A. (1998) Validation of Protein Structure from Anisotropic Carbonyl Chemical Shifts in a Dilute Liquid Crystalline Phase, *J. Am. Chem. Soc. 120*, 6836−6837.
55. Dyson, H. J., Tennant, L. L., and Holmgren, A. (1991) Proton-Transfer Effects in the Active-Site Region of *Escherichia coli* Thioredoxin Using Two-Dimensional ^{1}H NMR, *Biochemistry 30*, 4262−4268.
56. Koradi, R., Billeter, M., and Wüthrich, K. (1996) MOLMOL: A Program for Display and Analysis of Macromolecular Structures, *J. Mol. Graphics 14*, 51−55.
57. Jeng, M.-F., Campbell, A. P., Begley, T., Holmgren, A., Case, D. A., Wright, P. E., and Dyson, H. J. (1994) High-Resolution Solution Structures of Oxidized and Reduced *Escherichia coli* Thioredoxin, *Structure 2*, 853−868.
58. DeLano, W. L. (2002) *The PyMOL Molecular Graphics System*, DeLano Scientific, San Carlos, CA.

BI0508136